Hindawi
Advances in Materials Science and Engineering
Volume 2022, Article ID 7013748, 18 pages
https://doi.org/10.1155/2022/7013748

Research Article

Experimental Study on Mechanical Properties of Polypropylene: Steel Fiber Concrete and Loading Characteristics of Shaft Lining

Bendong Qin,[1] Shuo Li,[1] Jiaqi Guo ,[1] Shaofeng Liu,[1] Xiliang Liu,[1] Yongbiao Lai,[2] and Hailiang Li[3]

[1]*School of Civil Engineering, Henan Polytechnic University, Jiaozuo 454003, China*
[2]*China Construction Railway Investment Construction Group Ltd., Beijing 102601, China*
[3]*CCCC-SHEC Fourth Highway Engineering Co., Ltd., Luoyang 471013, China*

Correspondence should be addressed to Jiaqi Guo; gjq519@163.com

Received 9 September 2021; Revised 23 March 2022; Accepted 26 March 2022; Published 25 April 2022

Academic Editor: Akbar Heidarzadeh

With the rapid consumption of shallow coal resources, the depth of shaft lining construction continues to increase; huge formation pressure and complex geological conditions make the stress condition of shaft lining become more complex. The concrete strength grade is usually enhanced to improve the bearing capacity of shaft lining; however, high strength grades bring high brittleness. In order to solve the problem of high brittleness of high-strength concrete shaft lining in ultra-deep mine construction, a steel-polypropylene hybrid fiber high-performance reinforced concrete (SPHFRC) shaft model was developed. The SPHFRC with various mix proportions was prepared by optimizing the fiber content. The mechanical properties of SPHFRC were tested and compared with the reference concrete (PHSC). The results show that the SPHFRC can be obtained by adding the volume fraction in 1.2% steel fiber and 1.0% polypropylene fiber, which increases the tensile strength by 27.5% and the compressive strength of SPHFRC was similar to the reference concrete. By introducing a new brittleness evaluation index B to evaluate the brittleness of concrete, the results show the fiber greatly improves the brittleness problem of PHSC. Afterwards, a model test of PHSC and SPHFRC shaft lining was conducted, and the circumferential and axial load-stress-strain curves and load-displacement curves of concrete and steel bars are analyzed. Combining the failure characteristics of the two shaft lining models, the following conclusions are obtained: The ultimate bearing capacity of PHSC shaft lining is hardly affected by fibers, but the hoop displacement is significantly reduced and the circumferential stability of shaft lining has been greatly improved, the initial cracks appeared late, the speed of crack's propagation is reduced, and no obvious concrete peeling and separation appeared during damage. The comprehensive performance of SPHFRC shaft lining is excellent, which has better ductility and anti-deformation ability.

1. Introduction

China's energy structure is affected by the occurrence characteristics of poor oil, less gas, and rich coal energy. Coal has always occupied a dominant position in Chinese energy structure, so the sound development of coal industry is the premise of Chinese economic development. Less than 27% of China's coal resources are buried at a depth of 600 m, and about 53.2% of the total reserves are buried at a depth of 1000–2000 m. With the gradual reduction or even exhaustion of shallow coal resources, the depth of underground mining is increasing, and growing mines will face severe deep mining problems. The construction of vertical shafts, which is the main passageway of coal resource mining, has been deepened continuously; it has already advanced to 1000 m [1]. Shaft is the main entrance and exit of the mine to the ground, as a throat project for lifting and transporting coal (or gangue), transporting personnel, materials and equipment, as well as ventilation and drainage during mine production; its depth will inevitably continue to increase as the depth of coal mining increases [2–4]. Huge formation pressure and complex geological conditions have brought unprecedented challenges to bearing capacity and stability of traditional strength grade concrete shaft lining. It often causes shaft lining break and water leakage in varying degrees, not only incurs several hundred million dollars of

funds for maintenance, reinforcement but also affects the normal production safety [5]. To avoid the shaft lining rupture accidents, ensure safety in production, and improve economic efficiency, it has important theoretical significance and application value to carry out research on SPHFRC shaft lining materials and shaft lining mechanics characteristic [6, 7].

Research on SPHFRC was first carried out in Norway in 1986, since then, Japan, the United States, Canada, France, and Germany have successively devoted themselves to research and development, but it mainly focuses on ground engineering, and relatively few researches have been carried out on PHSC shaft lining materials. The use of SPHFRC in coal mine shaft linings in China began in the mining area east of Jining in 2001. The concrete strength grade used in shafts has reached C60 in the main and auxiliary shafts of Henan Chengcun Coal Mine in 2002 and the main shaft of Shandong Jixi Coal Mine in 2003. In recent years, China has made breakthroughs in the use of C80–C120 SPHFRC for deep-frozen shaft lining in coal mines, and it has been successfully applied in Deep Alluvium Freezing Shaft Sinking projects such as Zhaogu No. 1 Mine and No. 2 mine of coking coal company of Henan Energy Chemical Group Coking Coal Company [5, 8]. The experimental study of high strength concrete shows that, when the concrete strength exceeds C60, with the increase of its strength level, the brittleness is obviously enhanced, and the shaft lining has the characteristics of sudden failure [9–11]. The high brittleness and sudden failure characteristics of PHSC shaft lining material have become a new factor influencing the stability of the deep shaft lining. Improving the toughness of PHSC shaft lining concrete materials has become the key to the research and design of deep shaft lining structures. Concrete reinforced with fibers is widely utilized to attain noticeable durability in structures, the research of SPHFRC shaft lining materials and the mechanics characteristic of shaft lining has been produced according to demand [12–15]. In terms of SPHFRC shaft lining materials, Liu et al. [16] studied the hysteretic-loop and plastic deformation characteristics and energy evolution mechanism of C70 steel fiber shaft lining concrete soil material under uniaxial loading and unloading. The results show that the C70 steel fiber reinforced concrete tends to be fuller and the capacity of energy dissipation is stronger. Yang et al. [17] prepared hybrid fibers and micro-expansion high-performance shaft lining concrete by adding 1.092 kg/m^3 polyvinyl alcohol fiber (PVA), 5 kg/m^3 imitation steel fiber (FST), and 32.8 kg/m^3 CSA expansive agent, the combination of which has the advantages of increasing the compressive strength by 8.96% and the splitting tensile strength by 28.2%. Zhou et al. [18] studied the energy rule, damage characteristics, and failure pattern of shaft lining steel fiber–reinforced concrete in simulated deep underground environments by means of an uniaxial hydraulic servo machine, acoustic emission equipment, and a split Hopkinson pressure, they found that long fibers can retard the development of cracks. Yao et al. Ref. [19] found that the compressive strength of HFRC was similar to the reference concrete, but the tensile and flexural strength of HFRC was 42.7% and 35.1% higher than that of the reference concrete through the mixing test data of two dosages of polyvinyl alcohol fiber and polypropylene plastic steel fiber. Zhou et al. [20] researched on the performance change of fiber-reinforced high-performance concrete and fiber-reinforced reactive powder concrete subjected to simulated coastal ultra-deep mine environments. In the mechanical properties of hybrid fiber concrete shaft lining, Yao [21] through model experiments, the characteristics of stress and strength of the steel fiber reinforced high strength concrete shaft lining is studied. And the steel fiber reinforced high strength concrete shaft lining is of better plastic characteristic. Cai et al. [22] analyzed the causes affecting the mechanical characteristics of the steel fiber arc plate shaft lining through the test of shaft lining model and the FEM result shows that the steel fiber can improve the deformation and failure characteristics of the shaft lining. Yao and Wang et al. [19, 23] conducted an analog simulation model test of SPHFRC shaft linings, the new type of shaft lining structure containing hybrid fibers exhibited plastic deformation characteristics under load, and then using the Finite Element Method to obtain the mechanical characteristics of the shaft lining structure.

SPHFRC shaft lining material has superior performance than single fiber concrete. However, the research and development of SPHFRC shaft lining materials and the research on the mechanical characteristics of the shaft lining force are still in the first stage. Although some scholars have studied the properties of concrete such as compressive strength, splitting strength, elastic modulus, bending strength, and Poisson's ratio [24–26], the outstanding problem is that the optimal fiber content of SPHFRC shaft lining material is not clear and the mechanism of destruction is unknown. The bearing capacity and failure characteristics of SPHFRC shaft lining have not been fully revealed. In this paper, the mechanical properties and loading characteristics of shaft lining material of SPHFRC with outstanding performance-to-price ratio are studied. It is proposed to carry out compression and splitting tests and model tests of shaft lining's bearing capacity based on a series of concrete cube specimens. This paper carried out multi-angle analysis of compressive strength, tensile strength, brittleness index, and failure characteristics, given the optimum content of steel fiber and polypropylene fiber. Through analysis of shaft lining bearing capacity, axial and circumferential displacement, steel bar strain characteristics, dynamic development process of shaft lining cracks, and failure stage of shaft lining between PHSC and SPHFRC, this article reveals the internal mechanism of the difference in the failure characteristics of the two concrete shaft linings and the excellent performance of high-performance hybrid fiber concrete materials. The research results are of great significance to promoting the engineering application of SPHFRC shaft linings and to ensure the safety of deep shaft linings.

2. Mechanical Performance Tests of SPHFRC

2.1. Raw Materials. The materials used to prepare SPHFRC include: Cement: The production of P.O52.5R ordinary Portland cement of Henan MengDian Group Cement Co., Ltd

Table 1: Main properties of the P.O52.5R cement used in this study.

Chemical compositions of items	CaO	SiO_2	Al_2O_3	Fe_2O_3	MgO	SO_3	CL^-	Loss on ignition
	56.77%	20.86%	5.90%	3.61%	3.50%	2.43%	0.021%	1.16%
Physical properties property value	Specific surface area 381 m^2/kg		Initial setting 115 min	Final setting 184 min	3d compressive strength 33.8 MPa	28d compressive strength 58.6 MPa	3d flexural strength 6.2 MPa	28d flexural strength 10.7 MPa

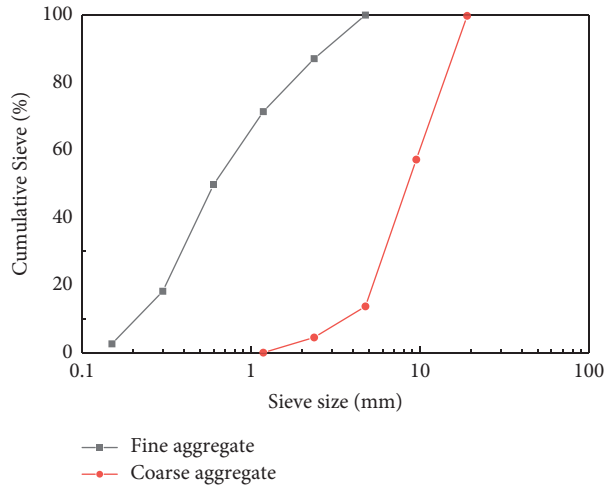

Figure 1: Sieve analysis of the used aggregate.

in compliance with Chinese national standardGB175-2007 [27] and its properties are presented in Table 1; The drinking water produced by Henan Jiaozuo water supply company meets the Chinese national standard GB5749-2006 [28]. There are few impurities in drinking water, which has no negative effect on the performance of concrete. The coarse aggregate: The particle size of 5 mm –20 mm of gravel, a continuous gradation, the specific gravity is 2.56, crushing index value of 7.8%–8%, and clean. The fine aggregate made of natural medium coarse river sand has a specific gravity of 2.62, fineness modulus of 2.6, particle gradation (0.2–4.75 mm), fineness modulus of 2.65, mud content of <1%, fine and coarse aggregate and were also utilized for grading (Figure 1) in compliance with Chinese national standards GB/T 14684-2011 [29] and GB/T 14685-2011 [30]. Composite mineral admixture: The Handan JunQiang Mining Technology Co., Ltd. JQ-HPC80 shaft of special additives, the content is the 10%–20% amount of cement (by mass); the basic physical and mechanical properties of steel fiber and polypropylene fiber (Zhengzhou, Henan) are shown in Table 2. The polypropylene fiber has a melting point of 160°C to 180°C, no water absorption, and acid and alkali resistance >96%. Polypropylene fiber and Steel fiber is shown in Figure 2.

2.2. Testing Methods and Equipment. The test method and operation process of this paper are under the standard for the test method of mechanical properties on ordinary concrete GBT50081-2002 [31] and GB50119-2013 [32]. Concrete cube compressive strength test adopts cube specimen with a side 150 mm (standard curing for 28 days). Test equipment in Figure 3 adopts the RMT-150B rock mechanics test system developed by the Wuhan Institute of Rock and Soil Mechanics, Chinese Academy of Sciences. The steel fibers and polypropylene fibers are difficult to dispersed uniformly and mixed in the concrete, so in this experiment with PVM500 compulsory mixer, we first put sand, cement, admixtures, and polypropylene fibers in the dry mix into a blender about 5 minutes, and after the polypropylene fibers are mixed, gravel, water, and steel fibers can be added.

The experiment of the concrete ratio which is the author deployment C70 high-strength concrete (concrete design results are shown in Table 3) in the lab early based on the mix by adding two different types of fibers and the fiber content was calculated by volume fraction. Steel fiber dosage range are 0.2%–1.2% to 0.2% increments, polypropylene dosage range is 0.05%–0.15% to 0.05% increments, mix design method of uniform design. Use S2P10F group and set an example which shows the symbol, S-steel fiber, P-polypropylene fiber, F-Fiber, 2-steel fiber dosage is 0.2%, and 10-Polypropylene dosage is 0.10%.

2.3. Testing Results and Analysis

2.3.1. Strength Properties. Using standard curing conditions and test methods, the 28-day compressive strength and split tensile strength of each sample was tested separately. There are three test samples for each group of mix ratios. The average strength values and strength ratios of the different mix ratio samples are shown in Table 4.

Table 2: Basic physical and mechanical parameters of fibers.

Fiber kinds	Fiber type	Length (mm)	Tensile strength (MPa)	Elastic modulus (GPa)	Density ($g \cdot cm^{-3}$)
Steel fiber physical and mechanical properties of fibers	Hook-type	35	>800	>200	7.8
Polypropylene	Monofilament	19	>560	>3500	0.91

Figure 2: Polypropylene fiber and steel fiber.

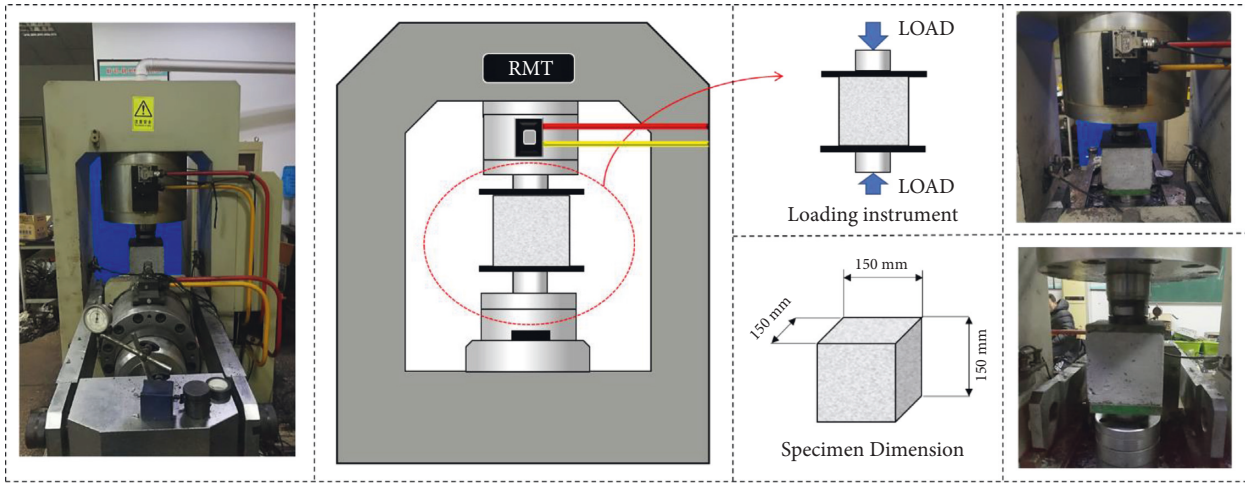

Figure 3: Experimental instruments.

Table 3: Mix proportions design kg/m^3.

Code	Cement	Water	Sand	Gravel	Admixture	m_a/m_b	Steel fiber (%)	Polypropylene fiber (%)
PHSC -1, 2, 3	460	148	655	1115	90	0.27	0	0
S2P10F-1, 2, 3	460	148	655	1115	90	0.27	0.2	0.10
S4P5F-1, 2, 3	460	148	655	1115	90	0.27	0.4	0.05
S6P15F-1, 2, 3	460	148	655	1115	90	0.27	0.6	0.15
S8P5F-1, 2, 3	460	148	655	1115	90	0.27	0.8	0.05
S10P15F-1, 2, 3	460	148	655	1115	90	0.27	1.0	0.15
S12P10F-1, 2, 3	460	148	655	1115	90	0.27	1.2	0.10

Note. m_a is water quality and mb is the quality of the cement and admixture.

Table 4: Strength properties of SPHFRC and PHSC.

Code	Slump (mm)	Compressive strength (MPa)	Compressive strength ratio	Splitting tensile strength (MPa)	Splitting tensile strength ratio	Tension and compression ratio
PHSC	210–220	79.60	1	4.18	1	0.0525
S2P10F	180–200	68.64	0.862	5.03	1.203	0.0733
S4P5F	180–200	86.54	1.087	5.19	1.241	0.0600
S6P15F	180–200	82.38	1.034	4.86	1.162	0.0590
S8P5F	180–200	75.87	0.953	5.30	1.267	0.0699
S10P15F	180–200	81.02	1.017	4.99	1.193	0.0616
S12P10F	180–200	78.05	0.980	5.33	1.275	0.0683

It can be seen from Table 4 that the compressive strength of the control group PHSC has reached 79.60 MPa at 28 days. It shows that the mix proportion of high strength concrete is effective. When the content of polypropylene fiber is 0.10%, the compressive strength increases with the increase of steel fiber content; when the content of polypropylene fiber is 0.05%, the compressive strength decreases with the increase of steel fiber content. It shows that the effect of hybrid fiber on the compressive strength of concrete is irregularly distributed. The compressive strength of some groups is slightly lower than that of the control group, and even lower than C70 (70 MPa) and "Negative confounding effect" appeared [33]. From Figure 4, we can see the six factors affecting the mechanical properties of concrete commonly used for evaluation are comprehensively considered. Mechanical properties of S12P10F group are better than other groups of hybrid fiber reinforced concrete.

Figure 5 shows the scatter diagram of compressive strength, splitting strength, and tension-compression ratio of concrete with different fiber content. It can be seen that after adding hybrid fiber, the tensile strength increases significantly, and the average value can reach 5.12 MPa. Compared with the experimental data table, it increased by nearly 22% compared with the control group. The tension-compression ratio of SPHFRC is higher than that of PHSC. The splitting tensile strength increases with the increase of steel fiber content. However, there was a relative decrease at 0.6% and 1.0% groups. According to the relevant research [34, 35], when only steel fiber is mixed with no more than 2.0%, the tensile strength should increase gradually. It shows a problem of optimal content of hybrid fiber, and it is not that the higher the content of hybrid fiber, the better the effect. Only by studying the optimal mix ratio can we give full play to the complementary advantages and cooperative working ability of the two kinds of fibers.

By analyzing the strength of SPHFRC with different fiber content, it can be seen that the strength of SPHFRC is greater or close to the PHSC, such as S10P15F, S12P10F, S6P15F, and S4P5F. The groups with less than 5% difference from the control group (79.6 MPa) were S12P10F, S10P15F, S8P5F, and S6P15F. S12P10F groups' splitting strength results are higher than the average (5.12 MPa), S8P5F, and S4P5F. There are two groups that are satisfied with both. They are S12P10F and S8P5F. But the S12P10F group has higher compressive strength and splitting tensile strength. The results show that the compressive strength of SPHFRC is similar to that of PHSC, but the tensile strength is 27.5% higher than that of reference concrete; this result is consistent with the mechanical properties of Yao and Yang's conclusion [17, 19].

2.3.2. Brittleness Properties. Figure 6 shows the complete compressive stress-strain curve of the concrete which has been tested, the rapid post-peak stress-strain curve of PHSC decreases faster than that of SPHFRC. Due to the rapid loss of bearing capacity, the testing machine cannot capture the complete stress-strain curve of the second half. The post-peak stress-strain curve of SPHFRC decreases more slowly than that of PHSC, and still has a certain bearing capacity after the peak. Comparing the SPHFRC with different doping amounts, we can see that the volume ratio of steel fiber has an obvious effect on the stress-strain curve of SPHFRC under uniaxial compression. With the increase of steel fiber volume ratio, the peak strain increases and the slope of the descending section decreases.

In this paper, the brittleness evaluation index based on energy is used to analyze the brittleness characteristics of concrete blocks under uniaxial compression. According to the uniaxial compressive stress-strain curve of concrete shown in Figure 6, the accumulation rate of pre-peak elastic property and the dissipation rate of post-peak elastic property are calculated, respectively. The representative regions of the store rate of prepeak elastic and the dissipation rate of post-peak elastic can be visualized in Figure 7. In figure 7, part S1 represents that when the concrete compression reaches the peak stress σ P, part of the energy generated by the external force is converted into irreversible dissipation energy. The other part is the elastic potential energy that can be recovered by accumulating in the concrete. The energy represented by the area of S_2 is shown in Figure 7. The brittleness of concrete can be characterized by the accumulation rate of pre-peak elastic potential energy, which is positively correlated with brittleness. When the concrete reaches the peak strength, it enters the breaking stage. The elastic energy accumulated in front of the peak provides part of the energy needed to overcome the destruction of internal cohesion and friction, the deficiency is provided by external mechanical energy. According to analysis, the post-peak fracture of concrete brittle materials is mainly provided by the elastic potential energy stored by itself. The greater the proportion of S_2–S_4, the higher the brittleness of $S_2 + S_3 - S_4$, which is the energy required for post-peak fracture energy. Therefore, according to the above analysis, the pre-peak and post-peak brittleness evaluation index is as follows:

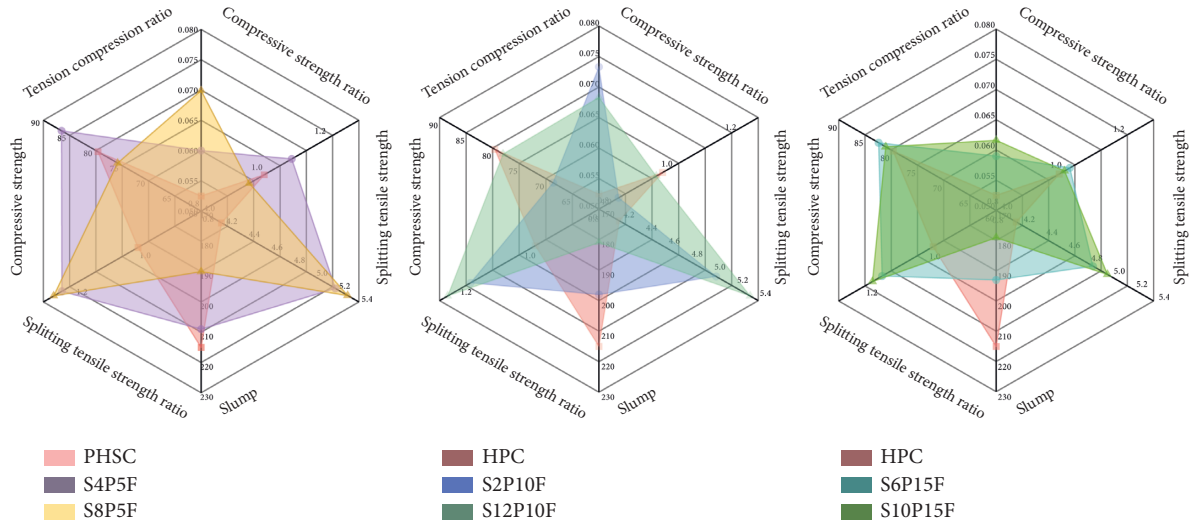

Figure 4: Comparison of the factors affecting the strength of different ratios.

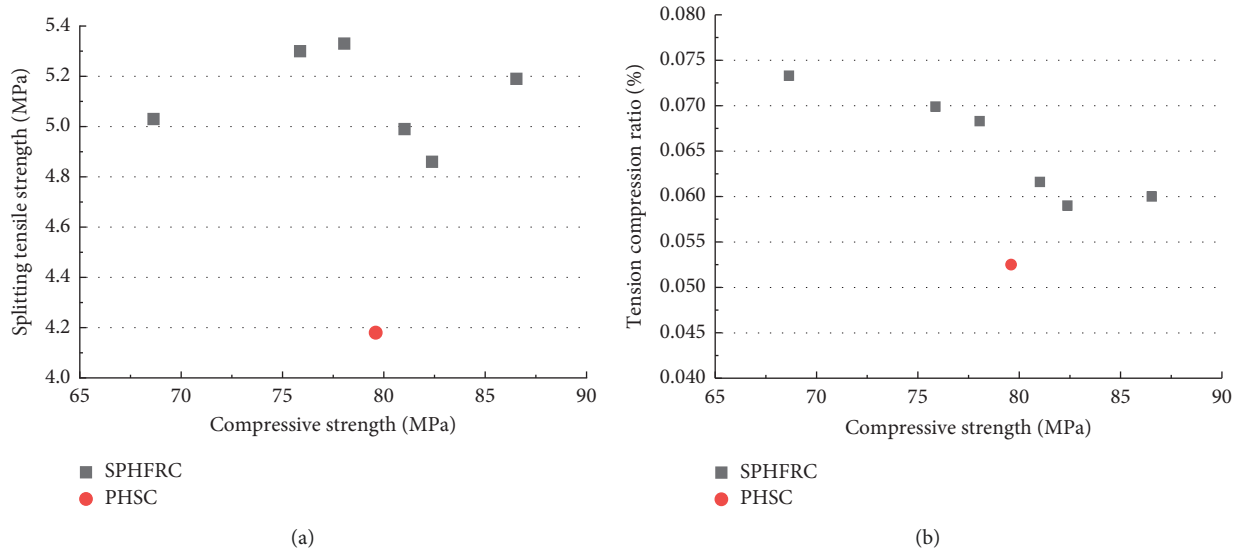

Figure 5: Effect of different fiber content on mechanical properties of concrete. (a) Effect on strength. (b) Effect on tension-compression ratio.

The pre-peak brittleness index can be calculated according to the following formula [36]:

$$BE_{\text{pre}} = \frac{S_2}{S_1 + S_2}. \tag{1}$$

In the formula: S_2 represents the pre-peak elastic performance; S_1 means that the dissipative energy is equal to the pre-peak mechanical energy W_{pre} minus the pre-peak elastic performance S_2. Among them: W_{pre} is obtained by integral calculation of stress-strain curve; $S_2 = \sigma_p^2/2E$ [37].

The post-peak brittleness index can be calculated according to the following formula [36]:

$$BE_{\text{post}} = \frac{S_2 - S_4}{S_2 + S_3 - S_4}. \tag{2}$$

In the formula: S_3 represents the mechanical work increment of rock caused by post-peak external force to maintain the post-peak fracture behavior of rocks, S_4 represents the residual elastic property of rock when it is in the state of residual stress; $S_4 = \sigma_r^2/2E$ [38]; as the whole process of evaluating the brittleness characteristics of concrete test, the brittleness index can be calculated according to the following formula [36]:

$$\text{B} = \frac{1}{2}\left(BE_{\text{pre}} + BE_{\text{post}}\right). \tag{3}$$

Brittleness index B is between 0 and 1. For ideal brittle materials $BE_{\text{pr}} = BE_{\text{pos}} = 1$, $B = 1$; For perfectly plastic materials $BE_{\text{pre}} = BE_{\text{pos}} = 0$, $B = 0$; the higher the value of B, the higher the brittleness.

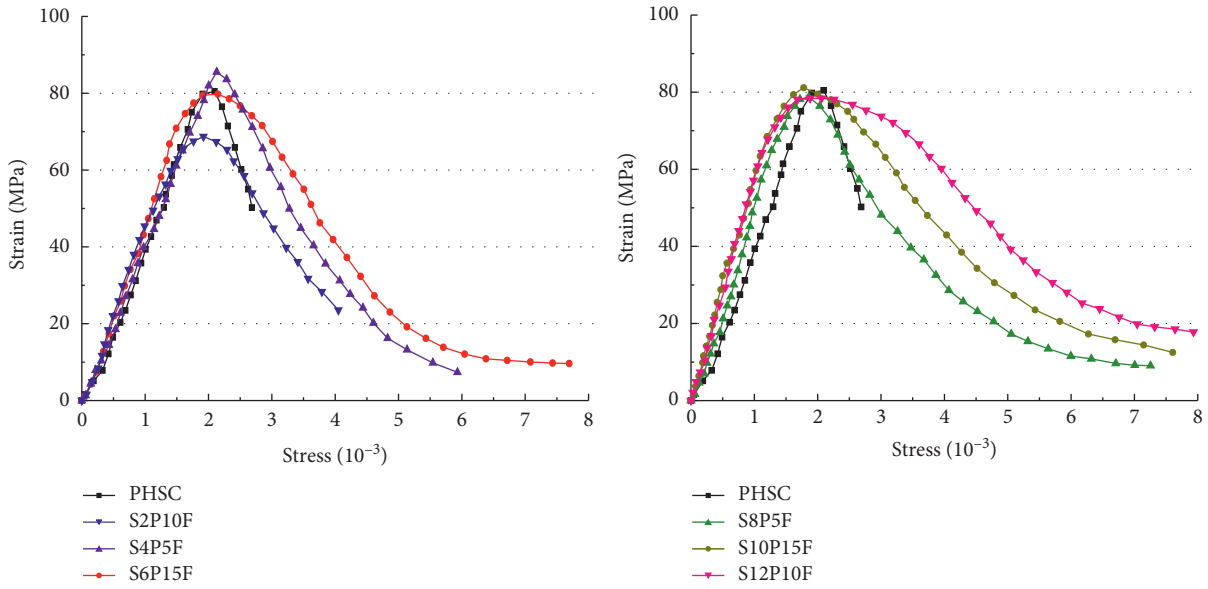

Figure 6: Comparison of SPHFRC and PHSC compressive stress-strain curves.

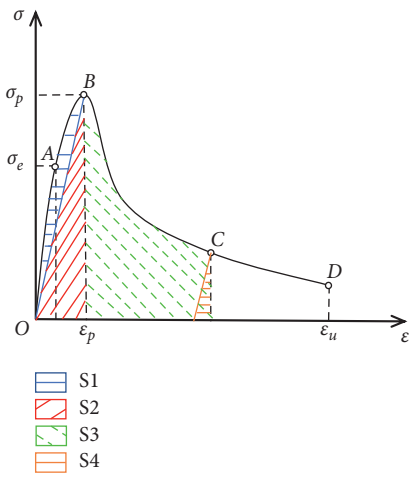

Figure 7: Pre-peak and post-peak energy changeover.

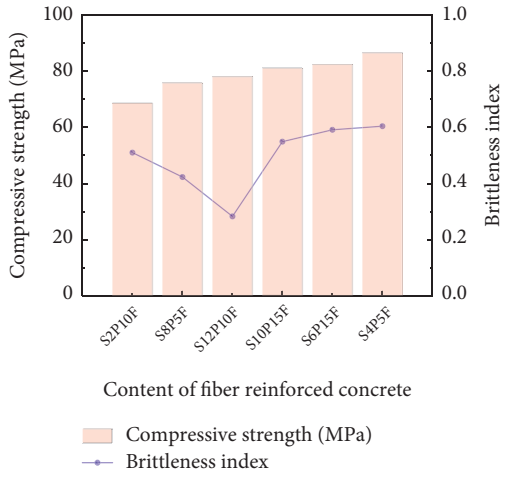

Figure 8: Comparison of brittleness index B.

Generally, the brittleness of specimens is proportional to the high strength of concrete. The result of calculating the brittleness index of each sample of SPHFRC is shown in Figure 8. It can be seen from Figure 8 that doped fiber can effectively improve the brittleness of concrete, in which BS12P10F is the smallest and has better toughness; this result is in good agreement with Deng' s research conclusion on toughness of hybrid fiber concrete [39]. As hybrid fiber reinforced concrete, the peak stress, peak strain, and toughness increase with the increase of steel fiber volume ratio. The content of fiber affects the brittleness index B of concrete, and the brittleness of concrete tends to be effective with the increase in fiber content. In the case of polypropylene fiber doped with the same volume fractional, increasing the content of steel fiber can improve the brittleness of concrete. BS12P10F is the smallest, so this group has better toughness. On this basis, comparing the strength of concrete with different fiber doping amount, under the condition of meeting the design strength, the concrete compressive strength of S12P10F group is increased by 13.71% and brittleness is reduced by 44.51% compared with S2P10F. Compared with S4P5F, the compressive strength is 8.49% lower, but the brittleness is 53.15% lower. Considering the influence of strength and brittleness of concrete, the S12P10F group is more advantageous.

2.3.3. Failure Properties. Failure under compression: The compression failure characteristics of some hybrid fiber reinforced concrete test blocks are shown in Figure 9. After the test block of the control group PHSC is loaded to 80% of the ultimate load, the failure characteristics of concrete have begun to become more and more obvious. It is characterized by a "pang-pang" sound inside the concrete. At the same

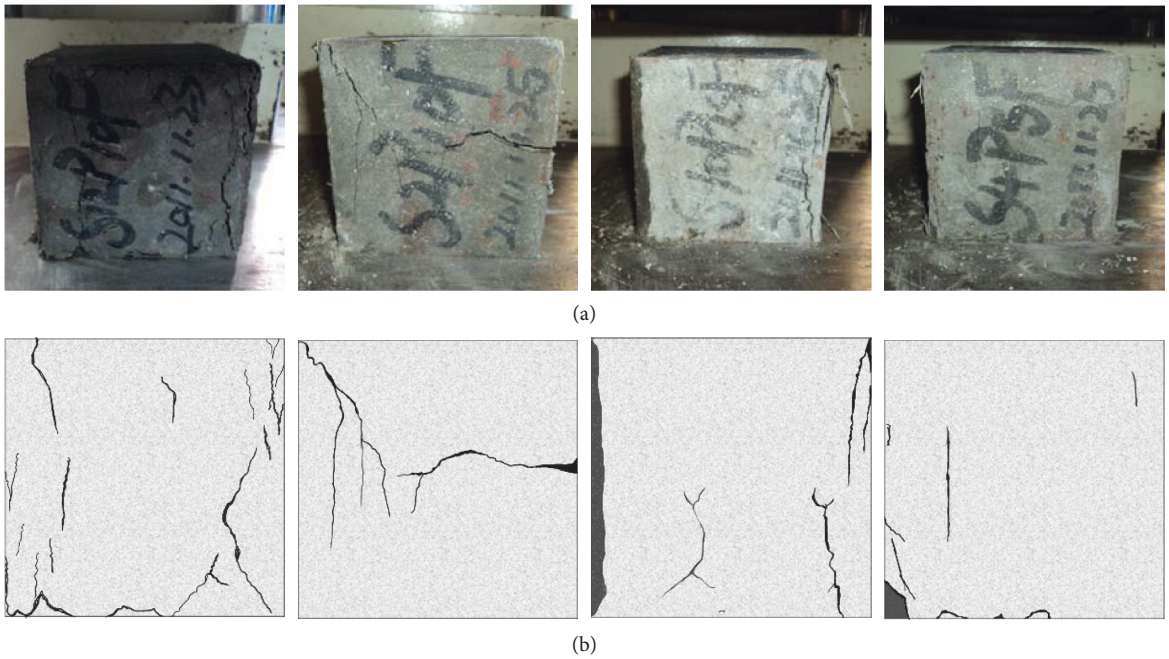

Figure 9: Characteristics of some test block splitting tensile failure. (a) Failure characteristics of SPHFRC test blocks under compression. (b) Description of cracks in SPHFRC test block.

time, the surface debris of concrete specimen fell in a large area. The test block is an inverted cone after the final failure. The specimens mixed with hybrid fibers do not have much fragments falling during the loading process, but there are some cracks on the surface of the specimens, which basically maintain their integrity after reaching the ultimate load. On the whole, the fiber produces a similar net binding force on the cracking and spalling of concrete, which makes the failure predictable and gradual, and shows good plastic characteristics. In order to facilitate observation, the crack description of hybrid fiber reinforced concrete test block is also given in Figure 9(b).

Failure under tensile: The failure characteristics of some test blocks are shown in Figure 10. In the loading process of the test block in the control group, there were no tensile cracks perpendicular to the backing plate. But when it is loaded to the ultimate load, it is accompanied by a "bang" sound, and the test piece breaks into two pieces without any sign. It can be seen that high-strength concrete has great brittleness. During the loading process of each test block mixed with hybrid fiber, macroscopically, there is no obvious debris falling, and it is not broken into two parts at the time of failure, so it still maintains a good integrity. There is only a main tensile crack along the middle of the test block. However, with different amounts of fiber in each group, the width and salience of cracks are also different. For example, in the high content S12P10F group, the macroscopic cracks are almost difficult to be detected by the naked eye. However, in the S4P5F group with lower content, the cracks can be clearly seen across the surface of the test block along the middle of the test block. It can be seen that doping hybrid fiber can improve the ductility of concrete and avoid the appearance of cracks too early. It has significant advantages in early crack resistance and improving brittleness.

This section systematically compares the mechanical parameters of two different concrete test blocks, SPHFRC and PHSC, such as compressive strength, tensile strength, tension-compression ratio, etc. Based on the brittleness index B defined by the energy principle, brittleness characteristics of SPHFRC with different doping amounts are analyzed. After studying the failure characteristics of two kinds of concrete test blocks, we decided to use S12P10F group mix ratio and use it as the fiber content of SPHFRC shaft lining to conduct model test on the stress and failure characteristics of shaft lining. Finally, the optimum fiber combination was determined as 1.2% (volume fraction) steel fiber and 0.1% (volume fraction) polypropylene in reference concrete.

3. Model Test of Mechanical and Failure Characteristics of Shaft Lining

In the second section, the mechanical properties of SPHFRC shaft lining materials are analyzed from the material level. The best fiber doping match of the SPHFRC shaft lining material is determined. It lays an important material foundation for improving the bearing capacity of deep shaft lining and ensuring the safety of the shaft lining. The shaft lining of deep shaft is an underground structure, and it is not enough to study it from the material level. In this section, through the model test of shaft lining bearing capacity of PHSC and SPHFRC, the characteristics of bearing capacity and failure characteristics of two kinds of concrete shaft lining are studied, and their internal mechanism differences are revealed.

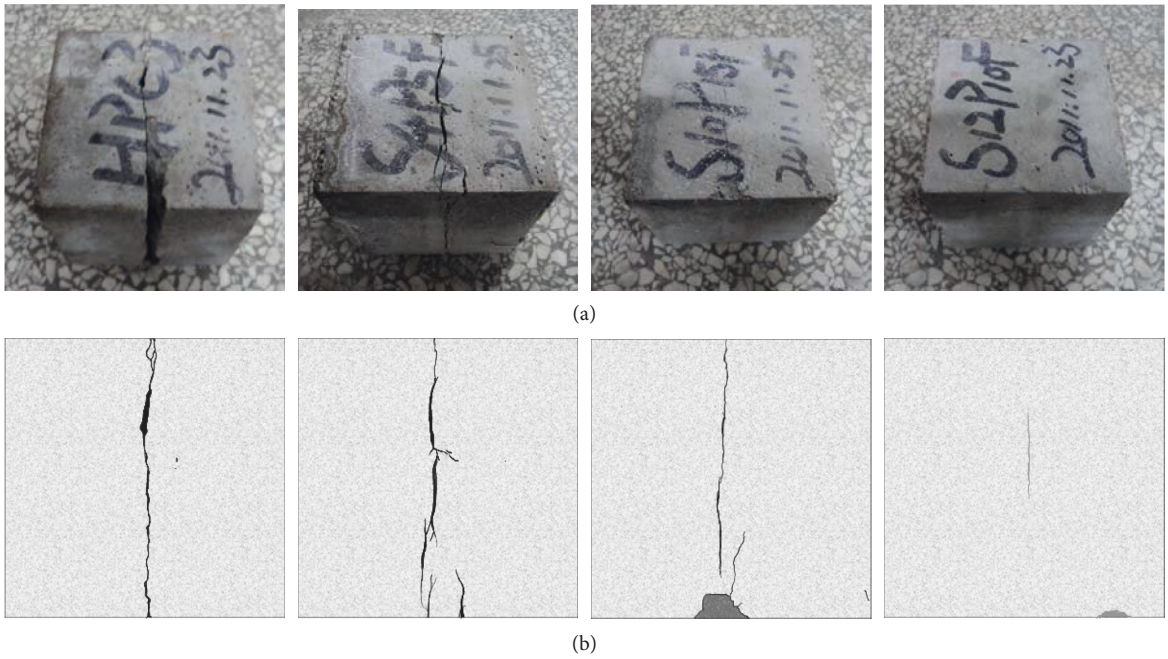

(a)

(b)

Figure 10: Characteristics of splitting and tensile failure of some test blocks. (a) Tensile failure characteristics of SPHFRC test blocks (including control group). (b) Description of cracks in SPHFRC test blocks.

3.1. Similarity Ratios of the Model Test. Due to the high strength and large geometric size of reinforced hybrid fiber-reinforced concrete shaft lining structure, it is difficult to carry out the failure test of prototype shaft lining. Therefore, the scaled shaft lining structure model is adopted in this paper. The purpose of this test is to obtain the loading characteristics of the shaft lining and the ultimate failure load. Therefore, shaft lining's design should not only meet the similar conditions of stress and deformation but also the similar conditions of strength. According to the similarity theory and the basic equation of elasticity, using the method of equation analysis [40], each similar index of the shaft lining needs to be determined, namely, Geometric similarity ratio C_l, Load similarity ratio C_p, Stress similarity ratio C_σ, Strain similarity ratio C_ε, Elastic modulus similarity ratio C_E, Poisson's ratio similarity ratio C_υ, Displacement similarity ratio C_δ. It can be obtained from the geometric equation: $C_\sigma/C_lC_\gamma = 1$; It can be obtained from the physical equation: $C_EC_\varepsilon = C_\sigma$, $C_\upsilon = 1$. In order to make the model test have practical generalization, if you want to be strictly similar to the prototype in load-deformation, you must ensure the model remains geometrically similar to the prototype before and after loading. $C_l = C_\delta$. Therefore, according to the above similar indicators, $C_\varepsilon = 1$. Therefore, the above stress and deformation conditions can be expressed by the following formula:

$$\frac{C_p}{C_\sigma} = 1, \quad \frac{C_EC_\varepsilon}{C_\sigma} = 1, \quad C_\upsilon = 1. \tag{4}$$

The materials used in the test are the same as the raw materials. Therefore, the stress-strain curve and the load-deflection curve of model material and prototype material are similar in the process of loading. At the same time, it should be similar to the strength, density, mechanical index, failure criterion, and other parameters of the prototype material. Therefore, it is necessary to satisfy the following formula:

$$C_\sigma = C_E = C_p = C_R = 1, \quad C_\mu = 1, \quad C_\rho = 1. \tag{5}$$

In the formula: Strength similarity constant C_R, Similarity constant of reinforcement ratio $C_\mu = 1$, Control similarity constant of steel fiber volume ratio $C_\rho = 1$. Under the condition of meeting the above similarity ratio, it is only necessary to determine the appropriate geometric similarity ratio. The model tests' results usually contains stress, strain, and displacement. The strain of the prototype is equal to that of the model, and the rest can be multiplied by the corresponding similarity ratio. The geometric similarity constant $C_l = 20$ in the model test, the detailed model size is shown in Table 5.

3.2. Preparation of Model Shaft Lining. Use the shaft model parameters in Table 4 to make the shaft model used in the test, the production process diagram is shown in Figure 10. When starting to pour, first make molds with plywood, PVC pipes, and resin glue as raw materials. The process of making the mold is shown in Figures 11(a)–11(c), then tie the steel cage and paste the strain gauge as shown in Figures 11(d)–11(g), binding reinforcement cage is based on Φ12 steel bar (Code for Design of concrete structures GB50010:2010). The strain gauge type is BX120-5AA, and the resistance value is $120 \pm 1\%$ (Ω). The circumferential steel bar pastes a strain gauge from top to bottom. The vertical steel bar pastes two

Table 5: Relevant parameters of original and model shaft lining.

Shaft	Internal diameter (mm)	External diameter (mm)	Shaft thickness (mm)	Height (m)	Reinforcement ratio (%)	Concrete grade
Prototype	5500	8300	1400	10	1.41	C70
Model	275	415	70	0.5	1.41	C70

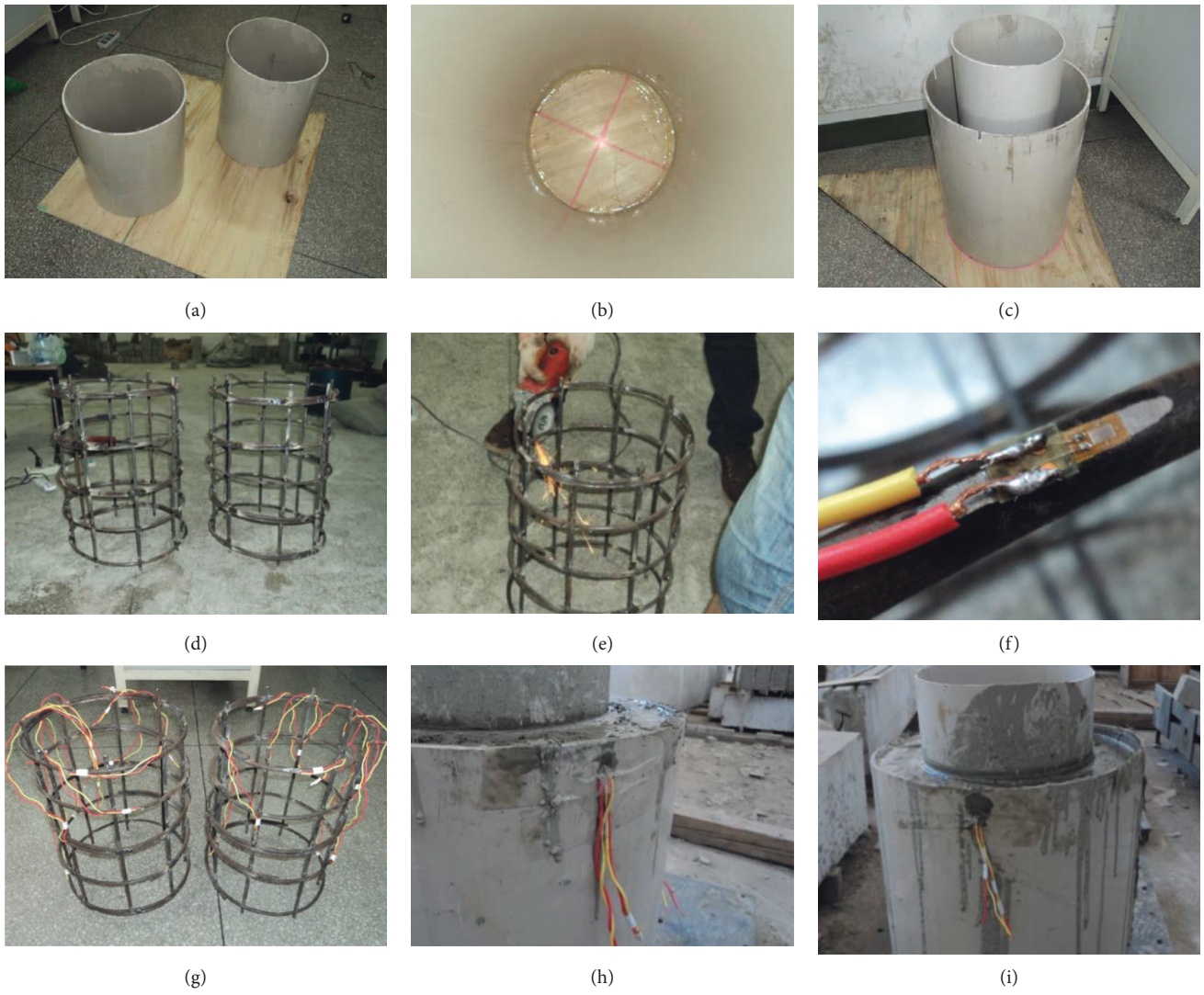

Figure 11: Preparation and pouring process of shaft lining. (a) Model raw materials. (b) Epoxy resin adhesive gluing result. (c) Shaft molds end product. (d) Shaft lining reinforcement model. (e) Reinforced grinding process. (f) Strain gauge paste results. (g) Shaft lining reinforcement model. (h) Details of the shaft lining placing. (i) Shaft lining placing results.

strain gauges symmetrically. In the process of pasting the strain gauge, it goes through the processes of polishing, alcohol cleaning, pasting, welding, and so on in strict accordance with the regulations. Then, the finished mold is placed in the center of the shaking table, the steel cage is placed in the mold, the internal wires are pulled out from the grooves cut on the mold, and the grooves are closed with waterproof glue. In the pouring process, 60 L forced mixer is used to mix the concrete. In pouring concrete, the upper and lower concrete cover of the steel bar is considered, so the 25 mm thick concrete should be poured at the bottom of the formwork, and then the steel cage should be slowly placed in the formwork. The method of layered vibration is used to make the interior of the specimen as uniform as possible. After all the pouring is completed, continue to vibrate for 5 min and continue to hit the outer surface of the mold with a rubber hammer as shown in Figures 11(h)-11(i). When pouring hybrid fiber reinforced concrete shaft lining and ordinary high strength concrete shaft lining, except that hybrid fiber reinforced concrete shaft lining needs to be doped with fiber, the operation of other parts should be strictly consistent. After the pouring of the specimen is

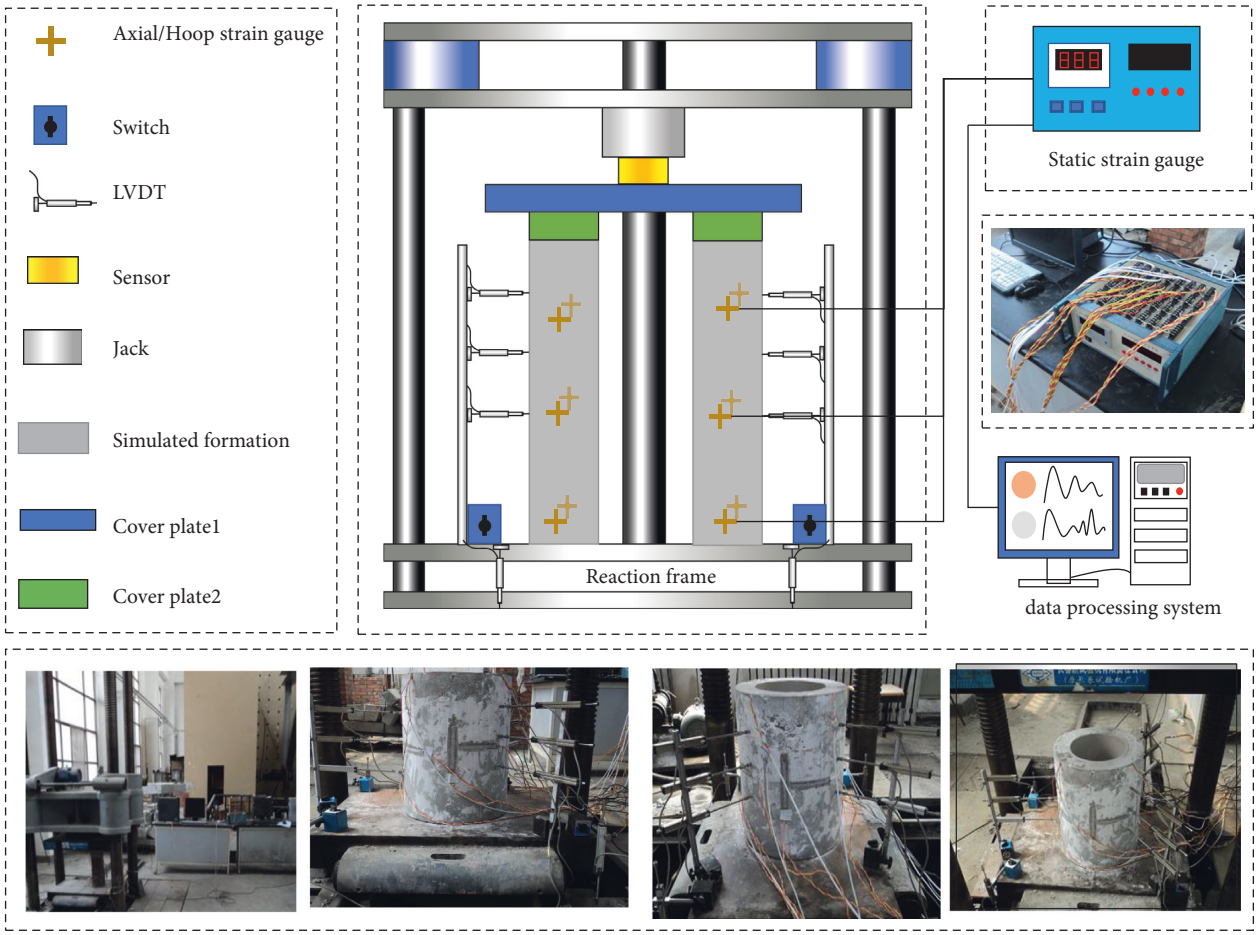

Figure 12: Experimental equipment and data acquisition device.

finished, it will be maintained under standard curing conditions for 28 days.

3.3. Testing Equipment and Methods. The loading device adopts 5000 kN microcomputer controlled electrohydraulic servo pressure testing machine produced by Changchun New testing Machine Co., Ltd. Displacement measuring device: the shaft lining axial displacement and radial displacement are measured automatically by the displacement meter. The strain recording device adopts that the strain of steel bar and concrete are measured automatically by static strain gauge, and the strain and displacement are automatically recorded by computer. Before the test, the two shaft linings are plastered separately in order to observe the cracks during the test. At the same time, the upper and lower surfaces of the shaft lining are polished to reduce the error caused by the eccentric compression of the shaft lining. Then the concrete strain gauge is pasted to the surface of the shaft lining. Along the middle surface of the shaft lining, the shaft lining is divided into four sections at an angle of 45°. Two strain gauges are pasted horizontally and vertically for each section, and a total of 8 concrete strain gauges are pasted. The test equipment and data acquisition device are shown in Figure 12. The test equipment was preheated before loading, and the specimen was subjected to a small loading-unloading operation within 0–10 kN for three cycles. The axial and radial displacement measurements of concrete are automatically recorded by computer, and the recording interval is 2000 ms. Control the loading speed to 100 N/s at 0–100 kN, and record the strain data every 10 kN. After that, the loading speed increases by 50 N every 30 s until it reaches 500 N/s. From now on, when loading to 2000 kN, the loading speed is controlled as 500 N/s, and data are recorded every other 50 kN. When the load exceeds 2000 kN, the loading speed decreases by 50 N every 30 s to 200 N/s, and at this speed until failure, the data are recorded every 10 kN.

4. Mechanical and Failure Characteristics of Model Shaft Lining

4.1. Loading Characteristic Analysis. Through the model tests of PHSC and SPHFRC shaft lining, the load-axial displacement curves and load-circumferential displacement curves of two kinds of concrete shaft lining are obtained, as shown in Figure 13. In order to facilitate the analysis, the load-displacement curve of concrete shaft lining is generally divided into four stages: the first stage OA is the concrete internal pore compaction stage; the second stage AB is the linear elastic deformation stage; the third stage is the crack formation stage to the stable expansion stage; and the fourth

stage CD is the crack unstable expansion to the loss of bearing capacity stage.

According to Figure 13, the main results are as follows:

(1) The ultimate compressive strength of ordinary high-strength concrete shaft lining model reaches 2175 kN, and the ultimate compressive strength of hybrid fiber high-strength concrete shaft lining model reaches 2250 kN, both of which are basically the same. The adulteration fiber does not affect the peak strength of high strength concrete shaft lining, has no negative effect on the bearing capacity of high strength concrete shaft lining, and even increases the ultimate compressive strength of high strength concrete shaft lining to a small extent. This conclusion is consistent with the previous mechanical test results of SPHFRC. The axial displacement increases linearly with the increase of compressive strength. Fiber doping shortens the length of the OA section in the diagram, reduces the compaction stage of the concrete, and makes the interior of the concrete denser by filling the fiber.

(2) At the initial stage of loading, the axial displacement increases greatly, which shows that the load-displacement curve increases in a small slope. When the radial displacement is about 1 mm, the load is only 100–150 kN. The main reason is that at the initial stage of loading, the smoothness of the shaft lining surface is relatively low, which requires a certain degree of load running-in period between the shaft lining surface and the bearing plate, resulting in excessive axial displacement at the initial stage of loading. In the elastic stage, comparing the AB section of the load-displacement curve of the shaft lining, we can see that the slope of hybrid fiber reinforced concrete is higher than that of ordinary high-strength concrete, indicating that the load-bearing capacity of hybrid fiber reinforced concrete is better than that of ordinary high-strength concrete. In the plastic fracture stage, the bearing capacity of the two shaft lining models decreases, showing that the radial displacement increases and the load increases.

(3) The circumferential displacement of the two kinds of concrete shaft lining increases with the increase of load, but when the circumferential displacement is the same, it can be seen that the axial pressure of hybrid fiber reinforced concrete is higher than that of ordinary high strength concrete. It shows that the overall performance of hybrid fiber reinforced concrete shaft lining is better in the process of loading. When the two kinds of concrete shaft lining are loaded to 2100 kN or so, the circumferential displacement of concrete begins to increase gradually, and finally when it is loaded to D point, the circumferential displacement of concrete shaft lining loses its bearing capacity and suddenly increases its fracture failure.

Figure 14 Load-strain relationship curves of circumferential steel bar and axial steel bar in the shaft lining of two kinds of concrete models. As can be seen from Figure 14, the main results are as follows:

(1) The strain regularity of circumferential steel bar in the two kinds of shaft lining models is significant, and they all rise in parabola. The characteristic of the rising section of the parabola is that the increment of the y-axis is much larger than that of the X-axis. It means in the initial compaction stage of this test, the strain of the steel bar develops little and is in the elastic stage, at the same time, the load increases sharply at this stage. When the load is 1000 kN, the strain begins to increase, indicating that the steel bar gradually enters the yield stage. Because of the "bridging effect" of two kinds of fibers in the hybrid fiber reinforced concrete shaft lining, the circumferential strain of the shaft lining is larger under the same load increment. Under roughly the same ultimate load, the circumferential strain of hybrid fiber reinforced concrete shaft lining is 70% higher than that of ordinary shaft lining. It shows that the fiber doping can significantly improve the circumferential stress state of the shaft lining.

(2) The longitudinal reinforcement strain of two kinds of shaft lining models increases with the increase of load. The load-strain curves of the longitudinal reinforcement of the two kinds of concrete shaft lining have no obvious yield point, indicating that when the shaft lining reaches the ultimate compressive strength, the concrete is crushed and peeled off, but the longitudinal steel bar does not reach its yield point, that is, the main reason for the failure of reinforced concrete shaft lining is the crushing failure of concrete, and the effect of steel bar on the bearing capacity of concrete is small.

Figure 14 shows the circumferential and axial load-strain curves of the shaft lining of two kinds of concrete models. As shown in Figure 15, the main results are as follows:

(1) The strain of circumferential and axial concrete increases with the increase of load, and the circumferential strain of hybrid fiber reinforced concrete is lower than that of ordinary high strength concrete, which indicates that the deformation of SPHFRC shaft lining is small and the overall performance is superior.

(2) The strain of circumferential concrete is much larger than that of axial concrete. Combined with the cracking and failure characteristics of the shaft lining in the loading process, it is shown that the part where the shaft lining is prone to fracture is in the middle of the shaft lining. The fracture mode is circumferential concrete cracking and spalling. The regularity of axial load-strain curve of a PHSC shaft lining is basically the same as that of hybrid fiber reinforced concrete shaft lining, which shows that hybrid fiber

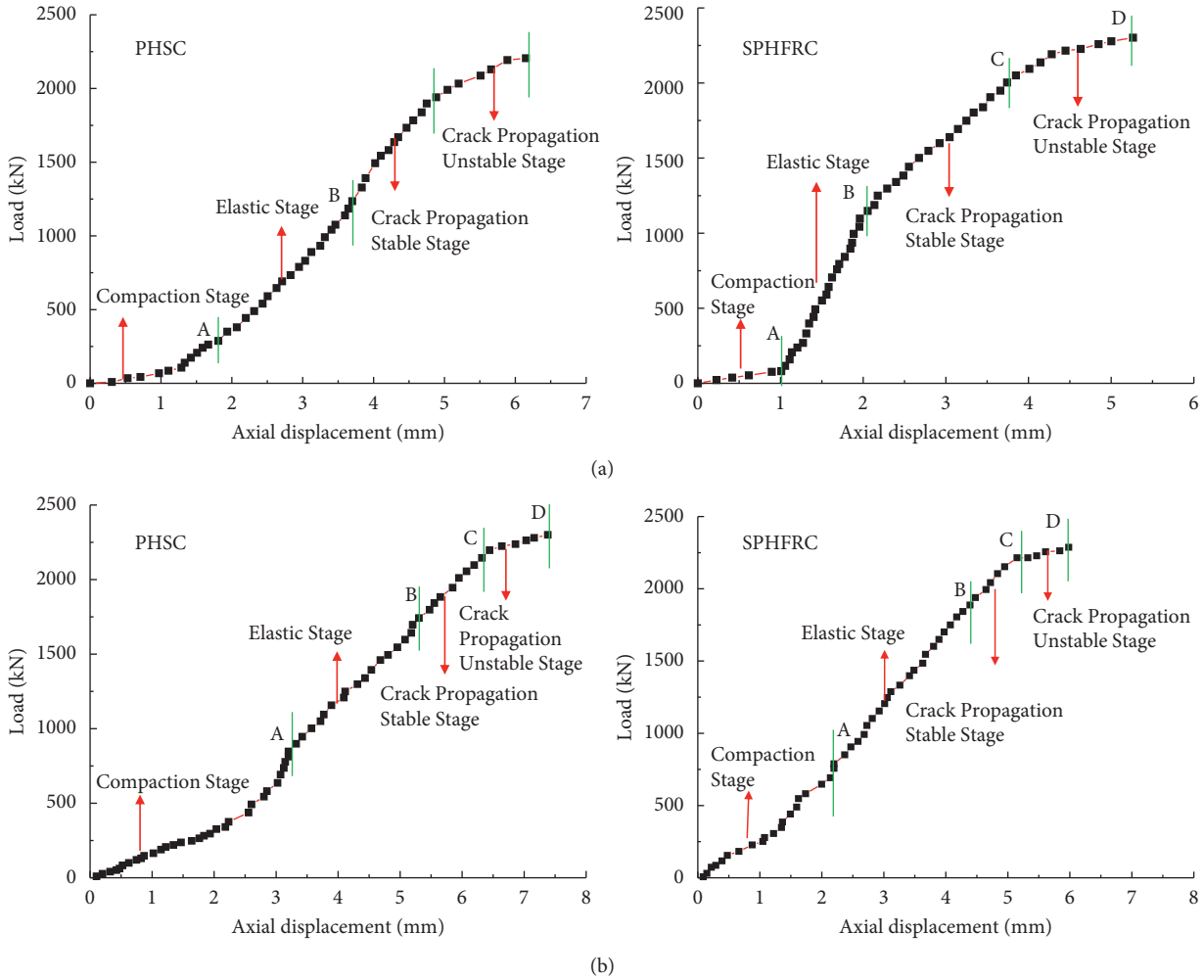

Figure 13: Load-displacement curve of model shaft lining. (a) Load-axial displacement curve. (b) Load-circumferential displacement curve.

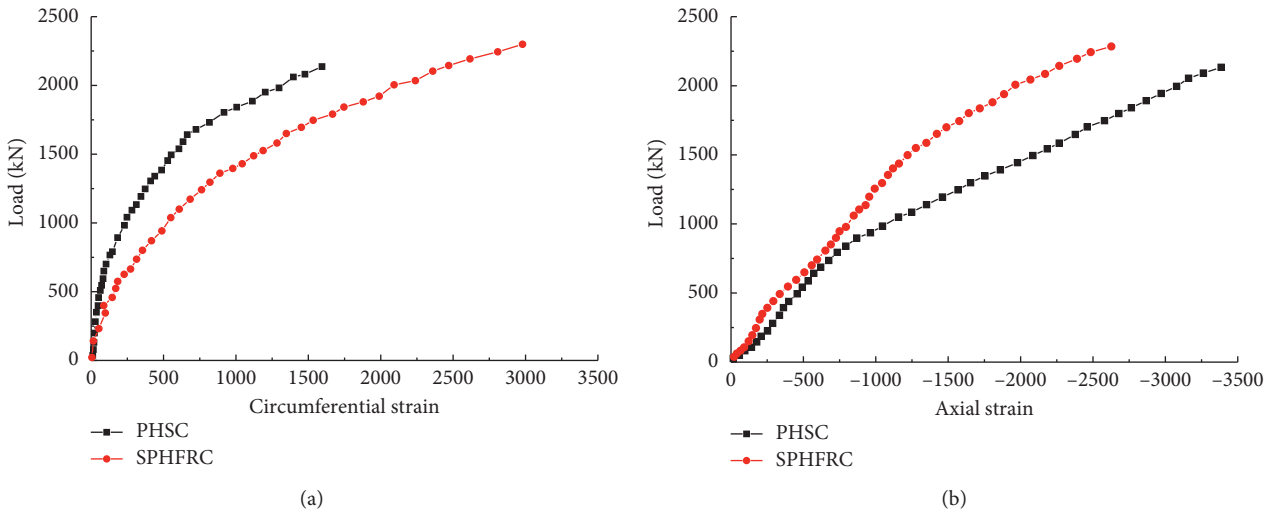

Figure 14: Load-strain curve of the steel bar in model shaft lining. (a) Load-circumferential strain curve. (b) Load-axial strain curve.

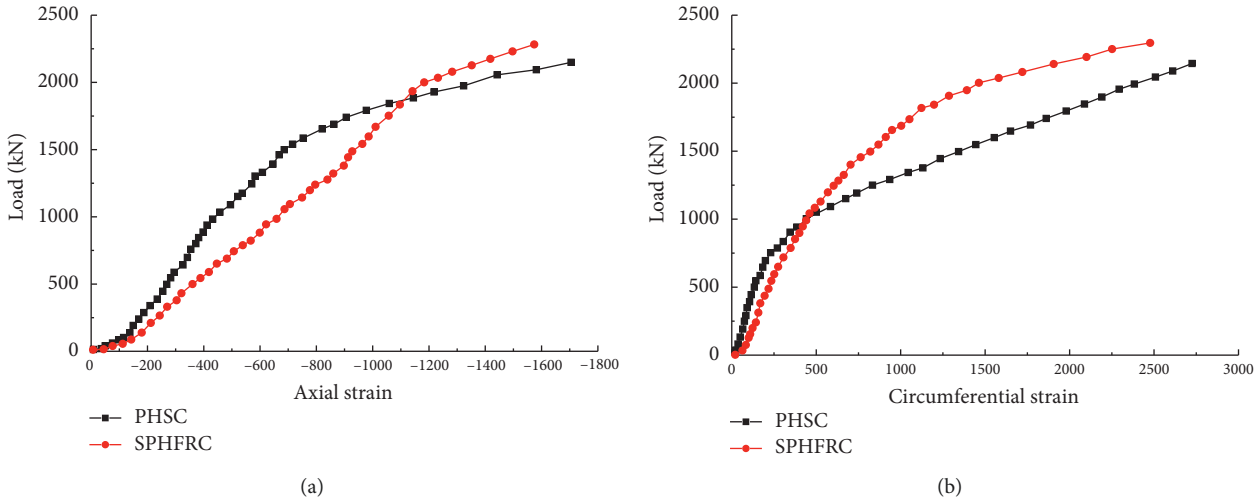

Figure 15: Load-strain curve of concrete in model shaft lining. (a) Load-axial strain curve. (b) Load-circumferential strain curve.

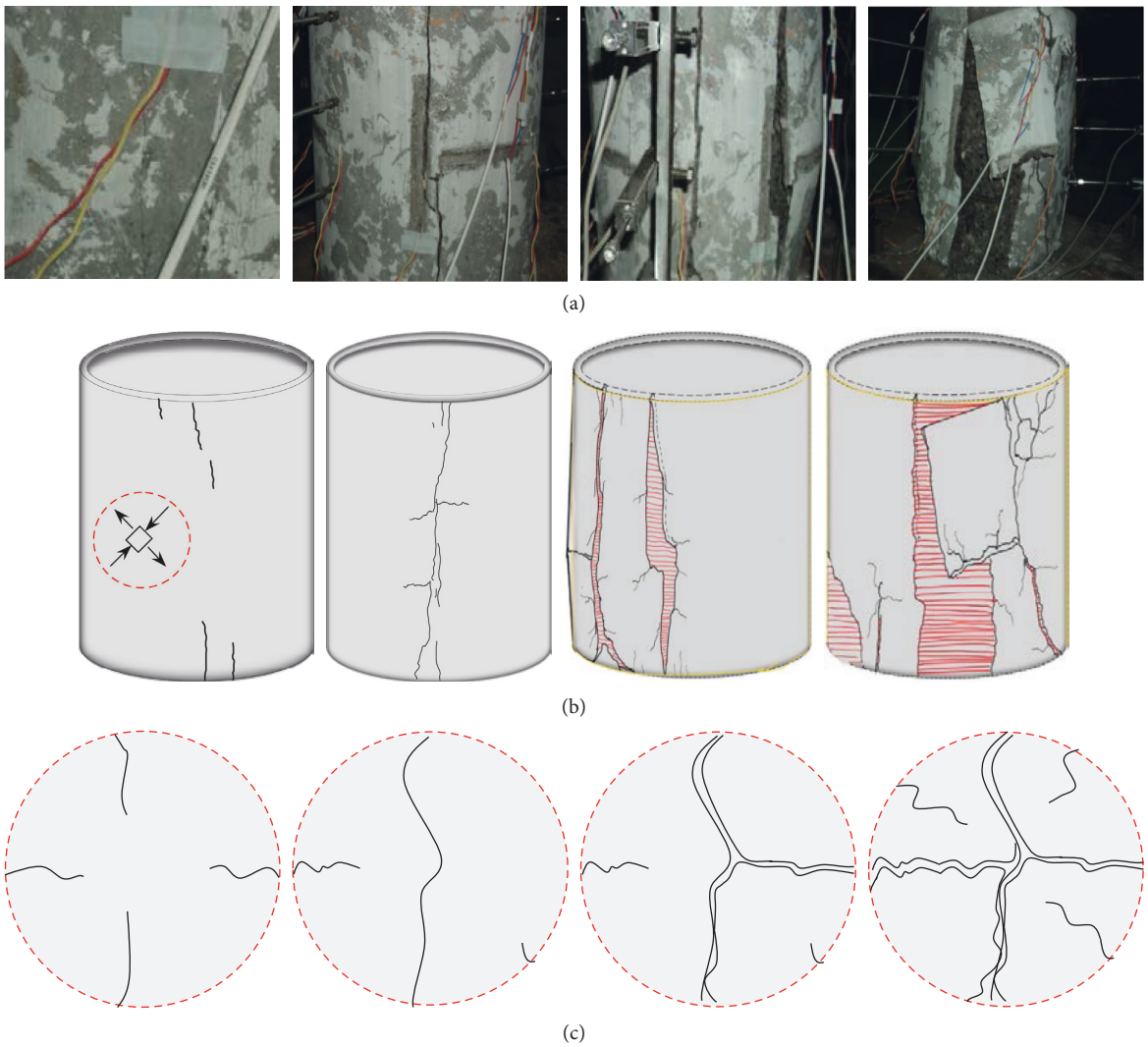

Figure 16: Macro and meso failure process of shaft lining of PHSC. (a) Real failure process of model shaft lining of PHSC. (b) Macroscopic failure process of model shaft lining of PHSC. (c) Microscopic failure process of shaft lining of PHSC.

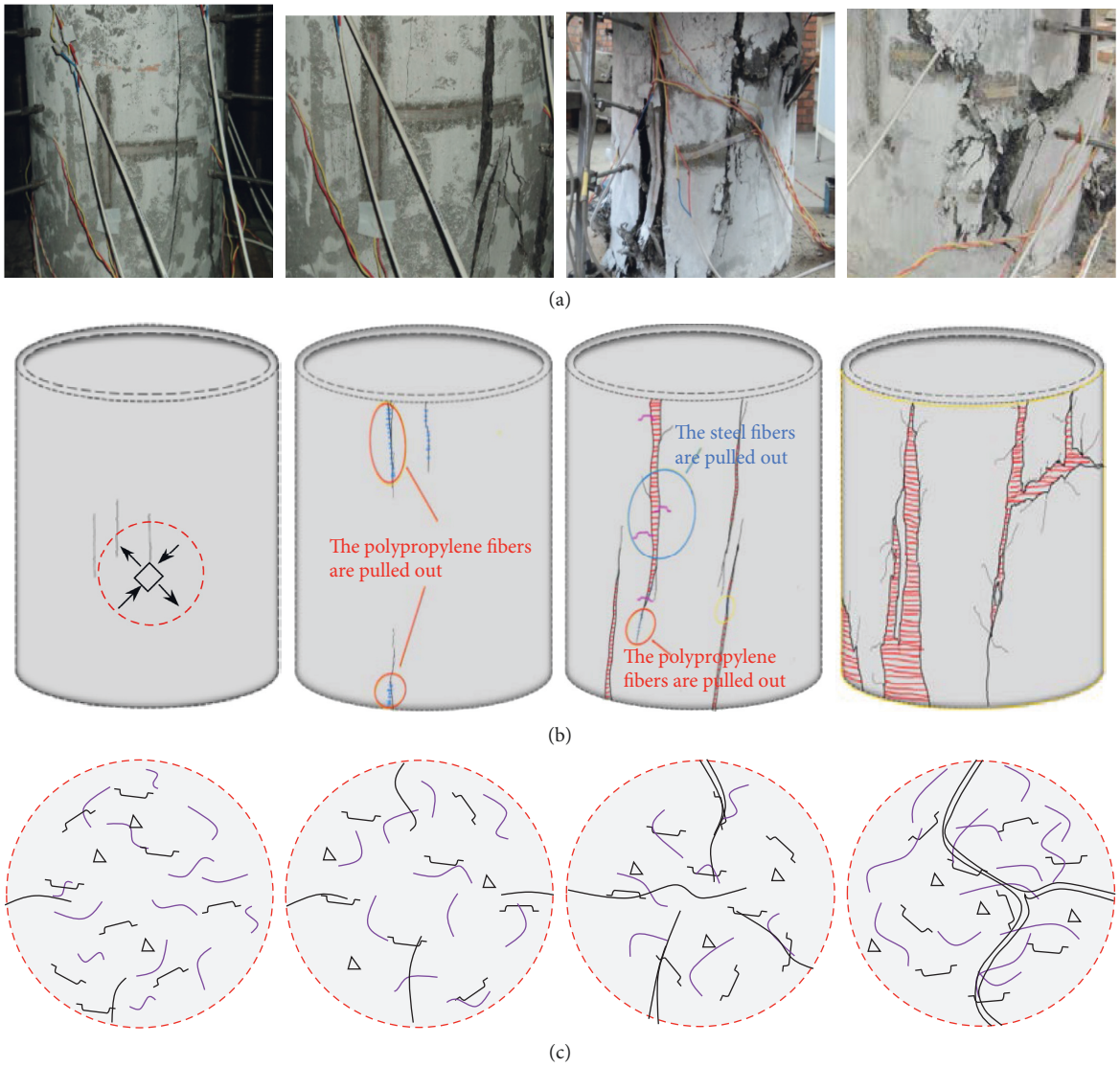

Figure 17: Macro and micro failure process of shaft lining of SPHFRC. (a) Real failure process of shaft lining of SPHFRC. (b) Macroscopic failure process of shaft lining of SPHFRC. (c) Microscopic failure process of shaft lining of SPHFRC.

has no obvious change on the axial strain of concrete under compression.

4.2. Analysis of Failure Characteristics of Shaft Lining

4.2.1. Failure Pattern of Shaft Lining of PHSC. The failure characteristics of ordinary high strength concrete shaft lining have gone through four stages: the appearance of micro-cracks, stable expansion of micro-cracks, crack penetration, and spalling failure of concrete. Figure 16 shows the failure process of hybrid fiber reinforced concrete shaft lining and the four steps of the stress state at a certain point in the process of macroscopic failure of ordinary high strength concrete shaft lining.

The fracture of ordinary high strength concrete shaft lining goes through the running-in between the initial loading model and the bearing plate. Micro-cracks along the axial direction of about 5 cm appear when the load reaches 600–700 kN, as shown in the first column of Figure 16. The cracks then widen with the increase of load; when the load reaches 1500–1600 kN, transverse cracks appear in the middle and lower part of the shaft lining, there are more evenly distributed end cracks at the bottom of the shaft lining, as shown in the second column of Figure 16. When the load reaches 1900 kN, the shaft lining cracks run through the shaft lining concrete bulging and a small amount of concrete peeling off as shown in the third column of Figure 16, but the shaft lining does not immediately fail, and the external bulging of the shaft lining model causes more cracks to run through. The steel bar inside the shaft lining protrudes when it is loaded above the 2100 kN, and a large area of concrete peels off as shown in the fourth column of Figure 16. The loading of the testing machine stops because of the sudden decrease in the bearing capacity of the shaft lining.

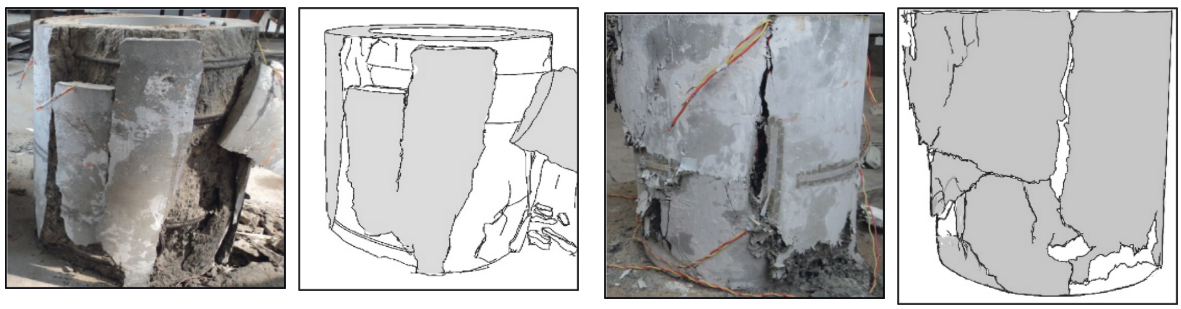

(a) (b)

Figure 18: Failure properties comparison of two model shaft linings. (a) PHSC. (b) SPHFRC.

4.2.2. Failure Pattern of Shaft Lining of SPHFRC. The failure process of hybrid fiber reinforced high strength concrete shaft lining goes through four stages: 1. microcrack initiation, 2. microcrack propagation (polypropylene fiber enhances the toughness of concrete), 3.microcracks continue propagation (polypropylene fiber toughness decreases and gradually withdraws from the work), 4. macrocrack occurrence, (steel fiber was pulled out and concrete was completely destroyed). Figure 17 shows the test failure process of the shaft lining model, and Figure 17 also shows the failure process of the shaft lining and the action mechanism of hybrid fibers in the shaft lining from both macro and micro angles.

Like ordinary high-strength concrete shaft lining, the hybrid fiber reinforced concrete shaft lining also experienced the running-in stage between the model and the bearing plate at the initial stage of loading. The difference is that the micro-cracks do not begin to appear until the load is 1000–1100 kN, as shown in the first column of Figure 17. At this stage, the tensile stress of the cracks is mainly borne by polypropylene fibers. As the load continues to be applied, the polypropylene fiber mixed in the concrete forms a network-like structure macroscopically, which limits the development of micro-cracks to a certain extent. With the increase of the internal stress of concrete, the hook structure at both ends of the steel fiber begins to play a certain anchoring role, and the steel fiber across the two ends of the crack begins to restrict the development of the initial crack and this is consistent with the discussion of the strength mechanism of steel fiber reinforced concrete by Liu et al. [16]. Different from the traditional shaft lining model, the location of the micro fracture in the shaft lining is more obvious in the middle part. When the load is up to 1600–1800 kN, the crack propagates gradually into the concrete matrix, the micro crack connects and runs through gradually, and the macroscopic crack appears. With the increase of the crack width, the polypropylene fiber reaches the ultimate tensile strength, and most of the polypropylene fiber withdraws from the work because of being pulled out, as shown in the second column of Figure 17. As the load continues to increase, when the tensile stress is greater than the accumulated bonding force between the steel fiber and the matrix, the steel fiber is pulled out as shown in the third column of Figure 17. After the load is loaded to 2000 kN, more and more steel fibers are pulled out, and the concrete without steel fiber bridge begins to peel off. Finally, a wide range of concrete cracks interweave to form a network of overall cracking, as shown in the fourth column of Figure 17, the bearing capacity decreases sharply, and the model is destroyed.

Both compression damage and tensile damage occur at the end of the column, and continue to develop along the initial damage, and finally form two oblique damage bands at both ends of the column. The failure characteristics of the model show that the reinforced concrete shaft lining is finally in shear failure state. When the reinforced concrete column is subjected to axial compression, although there is damage at the end of the column, the damage is mainly concentrated in the middle of the column as a whole; with the increase of load, the damage area in the column increases gradually, and several oblique damage bands are formed; then the damage zone continues to expand to form a main crack, and the deformation of reinforced concrete column increases; finally, the shear failure of reinforced concrete column occurs.

By comparison: the PHSC shaft lining is shown in Figure 18(a) Because of its poor ductility, there is no obvious sign before the damage, which is the sudden loss of bearing capacity. During the failure, there is a loud noise, with the spalling of a large piece of concrete, and the local concrete is crushed. The stress state of the concrete shaft lining is obviously improved by adding hybrid fiber, and the deformation of the specimen is restrained effectively. The model of SPHFRC shaft lining is shown in Figure 18(b), the spalling area of concrete is small and the amount of spalling concrete is small. The internal fiber delays the occurrence of cracks and deformation, and deformation capacity of the SPHFRC shaft lining model is improved, until the failure model still has a certain bearing capacity. Therefore, the use of hybrid fiber reinforced concrete in engineering application can greatly improve the deformation characteristics of shaft lining and improve the safety of the shaft lining engineering.

5. Conclusions

In this paper, the mechanical properties of SPHFRC and PHSC were studied systematically, and the stress and failure characteristics of PHSC and SPHFRC shaft lining are analyzed based on model tests. The main conclusions are as follows:

(1) By analyzing the mechanical properties of the hybrid fiber concrete test blocks with different mix ratios, combined with the brittleness evaluation index by the energy evolution method and the failure form of the concrete block, the results show that doping two kinds of fibers can significantly improve the peak of the concrete, post resistance, thereby significantly improving the ductility properties of hybrid fiber reinforced concrete. Doping $\varphi_V = 1.2\%$ steel fibers and $\varphi_V = 0.1\%$ polypropylene fibers can increase the tensile strength by 27.5%

(2) The bearing capacity test of the shaft lining shows that the bearing capacity of SPHFRC shaft lining is better than that of the PHSC group, indicating that adding hybrid fibers to the PHSC can meet the bearing capacity requirements. When the shaft lining is damaged, compared with the ordinary PHSC shaft lining, the SPHFRC shaft lining has a smaller circumferential displacement, a larger hoop strain of the steel bar, and a greater concrete hoop load-strain curve, indicating that the SPHFRC shaft lining has better toughness before failure and better integrity after failure.

(3) The circumferential displacement and strain of the shaft wall model are larger than the axial direction, and the damage is mainly the circumferential shear failure; the failure process of the PHSC shaft lining includes four stages: crack generation, crack propagation and connection, and outer bulge of the shaft lining, the large-area spalling section of concrete is mainly fracture damage, and the model will lose its integrity when it is damaged. While the failure of the SPHFRC shaft lining has 6 stages, namely, crack generation, crack propagation, polypropylene fiber pull-out, steel fiber pull-out, crack connection, and concrete spalling, there is no large area peeling, and the overall performance is better when damaged.

(4) The roles of the two fibers in the failure process of concrete are different. Polypropylene fibers have greater extensibility, which restricts the early shrinkage of concrete cracks and the early initiation of microscopic cracks. Under the action of low tensile stress, it will limit the development of cracks; once macroscopic cracks appear, polypropylene fibers will not work due to being pulled out, the steel fibers bridging both ends of the cracks play a anchoring role, restricting the development of macroscopic cracks. The two kinds of fibers mixed into concrete complement each other's advantages, and play a constraining effect on the expansion of concrete cracks at different stages, and enhance the toughness of the concrete.

Data Availability

The raw/processed data required to reproduce these findings cannot be shared at this time as the data also form part of an ongoing study.

Conflicts of Interest

The authors declare that they have no known competing financial interests or personal relationships that could have appeared to influence the work reported in this paper.

Acknowledgments

The authors are thankful for the financal support by the National Natural Science Foundation of China (nos. 51474097 and 51778215) and the Project Entrusted by the Enterprise (nos. H10-967 and H18-288).

References

[1] Q. S. Liu, W. Gao, and L. Yuan, *Stability Control Theory and Support Technology and Application of Rock Drift in Deep Coal Mine*, pp. 3–6, Science Press, Beijing, China, 2010.

[2] H. Zhang, G. S. Li, and S. Q. Jiang, "Time-space evolution pattern simulation experiment of surrounding rock deformation and destruction for superlilometer deep shaft roadway," *Journal of Experimental Mechanics*, vol. 33, no. 6, pp. 979–986, 2018.

[3] H. P. Xie, F. Gao, and Y. Ju, "Research and development of rock mechanics in deep ground engineering," *Chinese Journal of Rock Mechanics and Engineering*, vol. 34, no. 11, pp. 2161–2178, 2015.

[4] W. P. Xue, Z. S. Yao, W. Jingand, and H. Q. Song, "Mechanical damage and failure behavior of shaft-lining concrete after exposure to high pore-water pressure," *Journal of Materials in Civil Engineering*, vol. 32, Article ID 04019339, 2020.

[5] L. W. Jing, H. Zhang, H. D. Xu, and R. S. Yang, *Analysis of Shaft Deformation Mechanism and Study on Shaft Lining Material of High Strength and High-Performance concrete*, pp. 117–120, University of Science and Technology of China Press, Hefei, China, 2011.

[6] Z. S. Yao, Y. Cheng, and C. X. Rong, "Experimental study on composite shaft lining of innersteel plate cylinder and high strength reinforced concrete in deep frozen shaft," *Chinese Journal of Rock Mechanics and Engineering*, vol. 27, no. 1, pp. 153–160, 2008.

[7] L. Zhang, Y. Cong, H. Jiang, A. Erdiand, and Z. Wang, "Failure criterion for concrete shafts in deep alluvium zones based on plastic ultimate strain and its application," *Environmental Earth Sciences*, vol. 80, no. 5, pp. 1–16, 2021.

[8] X. G. Shi, C. F. Yang, and Y. J. Ding, "Application of high strength concrete C100 in freezing deep well," *Journal of Henan Polytechnic University (Natural Science)*, vol. 35, pp. 41–45, 2016.

[9] R. Zhou, H. Cheng, M. Li, L. Zhang, and R. Hong, "Energy evolution analysis and brittleness evaluation of high-strength concrete considering the whole failure process," *Crystals*, vol. 10, no. 12, p. 1099, 2020.

[10] T. Zhang, Y. Yin, Y. Gong, and L. Wang, "Mechanical properties of jute fiber-reinforced high-strength concrete," *Structural Concrete*, vol. 21, no. 2, pp. 1–10, 2020.

[11] N. H. Liang, X. R. Liu, and J. Sun, "Experimental study of crack resistance for multi-scale polypropylene fiber reinforced concrete," *Journal of China Coal Society*, vol. 38, no. 8, pp. 1304–1309, 2012.

[12] J. H. Haido, "Flexural behavior of basalt fiber reinforced concrete beams: Finite element simulation with new constitutive relationships," *Structures*, vol. 27, pp. 1876–1889, 2020.

[13] N. Banthia and R. Gupta, "Hybrid fiber reinforced concrete (HyFRC): fiber synergy in high strength matrices," *Materials and Structures*, vol. 37, no. 10, pp. 707–716, 2004.

[14] K. G. Kuder and S. P. Shah, "Processing of high-performance fiber-reinforced cement-based composites," *Construction and Building Materials*, vol. 24, no. 2, pp. 181–186, 2007.

[15] F. Deng, L. Xu, Y. Chi, F. Wu, and Q. Chen, "Effect of steel-polypropylene hybrid fiber and coarse aggregate inclusion on the stress-strain behavior of ultra-high performance concrete under uniaxial compression," *Composite Structures*, vol. 252, pp. 112685–112702, 2020.

[16] J. H. Liu, Y. C. Zhou, and H. G. Ji, "Energy evolution mechanism of shaft lining concrete under uniaxial loadingand unloading compression," *Journal of China Coal Society*, vol. 43, no. 12, pp. 3364–3370, 2018.

[17] L. Yang, Z. Yao, W. Xue, X. Wang, W. Kong, and T. Wu, "Preparation, performance test and microanalysis of hybrid fibers and microexpansive high-performance shaft lining concrete," *Construction and Building Materials*, vol. 223, pp. 431–440, 2019.

[18] Y. C. Zhou, J. H. Liu, H. T. Yang, and H. G. Ji, "Failure patterns and energy analysis of shaft lining concrete in simulated deep underground environments," *Journal of Wuhan University of Technology*, vol. 35, pp. 170–182, 2020.

[19] Z. Yao, X. Li, T. Wu, L. Yang, and X. Liu, "Hybrid-fiber-reinforced concrete used in frozen shaft lining structure in coal mines," *Materials*, vol. 12, pp. 1–13, 2019.

[20] Y. C. Zhou, J. H. Liu, S. Huang, H. T. Yang, and H. G. Ji, "Performance change of shaft lining concrete under simulated coastal ultra-deep mine environments," *Construction and Building Materials*, vol. 230, pp. 1–10, 2020.

[21] Z. S. Yao, "An experimental study on steel fiber reinforced high strength concrete shaft lining in deep alluvium," *Chinese Journal of Rock Mechanics and Engineering*, vol. 24, pp. 1253–1257, 2005.

[22] H. B. Cai, Z. S. Yao, and C. X. Rong, "Mechanical characteristic of steel fibre concrete arc shaft lining structure," *Journal of China Coal Society*, vol. 35, pp. 46–50, 2010.

[23] X. Wang, H. Cheng, T. Wu, Z. Yao, and X. Huang, "Numerical analysis of a novel shaft lining structure in coal mines consisting of hybrid-fiber-reinforced concrete," *Crystals*, vol. 10, no. 10, p. 928, 2020.

[24] J. H. Haido, B. A. Tayeh, S. S. Majeed, and M. Karpuzcu, "Effect of high temperature on the mechanical properties of basalt fibre self-compacting concrete as an overlay material," *Construction and Building Materials*, vol. 268, Article ID 121725, 2020.

[25] S. S. Majeed, J. H. Haido, and D. S. Atrushi, "Properties of self-compacted concrete incorporating basalt fibers: experimental study and Gene Expression Programming (GEP) analysis," *Computers and Concrete*, vol. 28, no. 5, pp. 451–463, 2021.

[26] J. H. Haido, S. T. Yousif, and A. A. Abdul-Razzak, "Dynamic response of reinforced concrete members incorporating steel fibers with different aspect ratios," *Advances in Concrete Construction*, vol. 11, no. 2, pp. 89–98, 2021.

[27] China Standards Publication, *Common portland Cement;GB 175-2007/XG1-2009*, Standard Press of China, Beijing, China, 2007.

[28] China Standards Publication, *Hygienic Standard for Drinking Water. GB 5749-2006*, Standard Press of China, Beijing, China, 2006.

[29] China Standards Publication, *Sand for Construction; GB/T 14684-2011*, Standard Press of China, Beijing, China, 2011.

[30] China Standards Publication, *Pebble and Gravel for Construction.GB/T 14685-2011*, Standard Press of China, Beijing, China, 2011.

[31] China Standards Publication, *Standard for Test Method of Mechanical Properties on Ordinary Concrete; GBT/50081-2002*, Standard Press of China, Beijing, China, 2002.

[32] China Standards Publication, *Code for Concrete Admixture Application; GB/50119-2013*, Standard Press of China, Beijing, China, 2013.

[33] J. Zhao, X. H. Cai, and H. J. Jiao, "Effect of hybrid fiber on early cracking behavior in concrete," *Journal of Harbin Institute of Technology*, vol. 39, pp. 232–234, 2007.

[34] X. Luo and W. Sun, Y. N. Chan and S. Y. N. Chan, Steel fiber reinforced high-performance concrete: a study on the mechanical properties and resistance against impact," *Materials and Structures*, vol. 34, no. 3, pp. 144–149, 2001.

[35] E. T. Dawood and M. Ramli, "Mechanical properties of high strength flowing concrete with hybrid fibers," *Construction and Building Materials*, vol. 28, no. 1, pp. 193–200, 2012.

[36] G. Q. Chen, J. C. Wu, W. Z. Jiang, S. J. Li, Z. B. Qiao, and W. B. Yang, "An evaluation method of rock brittleness based on the whole process of elastic energy evolution," *Chinese Journal of Rock Mechanics and Engineering*, vol. 39, pp. 901–911, 2020.

[37] H. P. Xie, Y. Ju, and L. Y. Li, "Criteria for strength and structural failure of rocks based on energy dissipation and energy release principles," *Chinese Journal of Rock Mechanics and Engineering*, vol. 24, no. 17, pp. 3003–3010, 2005.

[38] J. Zhang, C. Ai, Y. W. Li, J. Zeng, and D. Z. Qiu, "Brittleness evaluation index based on energy variation in the whole process of rock failure," *Chinese Journal of Rock Mechanics and Engineering*, vol. 36, pp. 1326–1340, 2017.

[39] Z. C. Deng, "Flexural toughness and evaluation method of hybrid fiber reinforced ultra-high-performance concrete," *Journal of Composite Materials*, vol. 33, pp. 1274–1280, 2016.

[40] C. C. Xia and Y. S. Li, *Testing Theory and Monitoring Technology of Underground Engineering*, Tongji University Press, Shanghai, China, 1999.